Beam-Plasma Interaction Experiments and Diagnostics*

I. ALEXEFF, R. V. NEIDIGH, AND W. F. PEED
Oak Ridge National Laboratory, Oak Ridge, Tennessee
(Received 8 June 1964)

Beam-plasma interaction is thought to heat ions and electrons. A deuterium plasma is trapped between magnetic mirrors and traversed by a 5-kV, $\frac{1}{2}$-A electron beam emerging from a highly ionized region in the mirror throat. The interaction amplifies the electron temperature of the plasma until the pressure exerted by the plasma competes with the pressure of the containing magnetic field ($8\pi nKTB^{-2}\approx 1$). Techniques used in measuring the density, temperature, and stability of the plasma are described.

INTRODUCTION

IN this report we describe a method of generating a hot-electron and warm-ion plasma by beam-plasma interaction,[1–3] and discuss the techniques used to measure its density, temperature, and stability. We measure its electron temperature from the bremsstrahlung x-ray energy spectrum. We deduce its density from the x-ray source strength and measure it independently by a neutral beam technique. We observe its stability by time analyzing the decay of its diamagnetism and x-ray flux. We infer its ion temperature from charge exchange and scattering laws. The paper first describes the apparatus and operation, then the experimental measurements, and concludes with some observations on stability.

APPARATUS AND OPERATION

An outline of the coils for producing the magnetic field and the cathode-anode for the electron beam are superimposed on the visible plasma of Fig. 1. Both the plasma and the electron beam were formed by a technique similar to that for the pressure gradient arc,[4,5] sometimes called mode II. Not shown in the outline is the gas feed into the beam-defining aperture in the anode, which produces a local high-pressure region of 10^{-3} to 10^{-2} Torr. Between the mirrors the pressure is reduced to 10^{-5} to 10^{-4} Torr by large-throughput diffusion pumps. Also not shown is an electrode (anticathode) for reflecting the electron beam. Its potential is not critical for interaction but has a "best value" for maximum electron temperature.

In the experiments to be described, the coil spacing is 7.5 in. center to center. The plasma volume, as indicated by the x-ray image, is about 100 cm^3. The diameter of the visible plasma at the midplane is about 3 in. even though the diameter of the electron beam which generated the plasma was limited in the mirror throat, and were it not for the interaction would be less than $\frac{1}{2}$ in. at the midplane. A tenuous plasma or bursts of plasma must extend beyond even this visible limit because of a ring of x-ray fluorescence which appears around the coil throat and gives a dumbbell-like appearance to the x-ray image of Fig. 1. Clearly, an extensive secondary plasma forms which extends beyond the initial collimation of the electron beam.

A current-limited power supply (with low-resistance load the voltage appears across a limiter tube) was used to bias the filament. This bias was -5000 V in most cases with 0.5-A drain on the power supply. The anticathode was self-biased, that is, its potential (-1000 to -2000 V) was determined by the value of its resistor to ground (usually about 3000 Ω).

The usual discharge tends to be of the low-power, high-current type with low resistance, little secondary plasma, and no interaction with the beam. However, as with an oscillator, interaction may be started by a

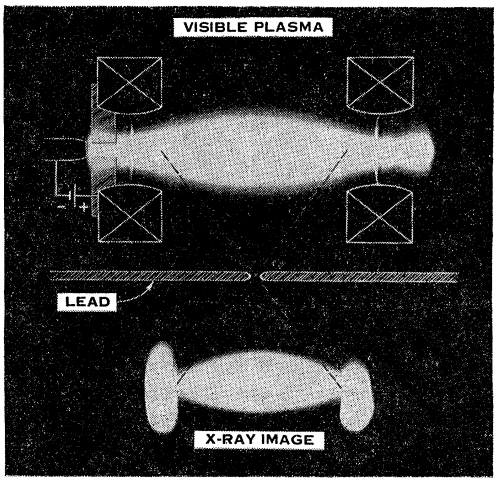

FIG. 1. Visible hot-electron plasma and its x-ray image. Superimposed outline shows magnet coils and electron-beam defining aperture. Dumbbell-like ends on the image are caused by x-ray fluorescence at the magnetic-mirror throat.

* Research sponsored by the U. S. Atomic Energy Commission under contract with the Union Carbide Corporation.

[1] L. D. Smullin and W. D. Getty, Phys. Rev. Letters **9**, 3 (1962); W. D. Getty, B. Hartenbaum, H. Hsieh, and L. D. Smullin, Bull. Am. Phys. Soc. 8, 169 (1963).

[2] I. F. Kharchenko *et al.*, Proceedings of the Salzburg Conference on Nuclear Fusion, Paper CN-10/230/A, Salzburg, Austria, 1961 (unpublished).

[3] Igor Alexeff, R. V. Neidigh, W. F. Peed, E. D. Shipley, and E. G. Harris, Phys. Rev. Letters **10**, 273 (1963).

[4] R. V. Neidigh and C. H. Weaver, *Proceedings of the Second United Nations International Conference on the Peaceful Uses of Atomic Energy, 1958* (United Nations, Geneva, 1959), Vol. 31, p. 315.

[5] Igor Alexeff and R. V. Neidigh, Phys. Rev. **129**, 516 (1963).

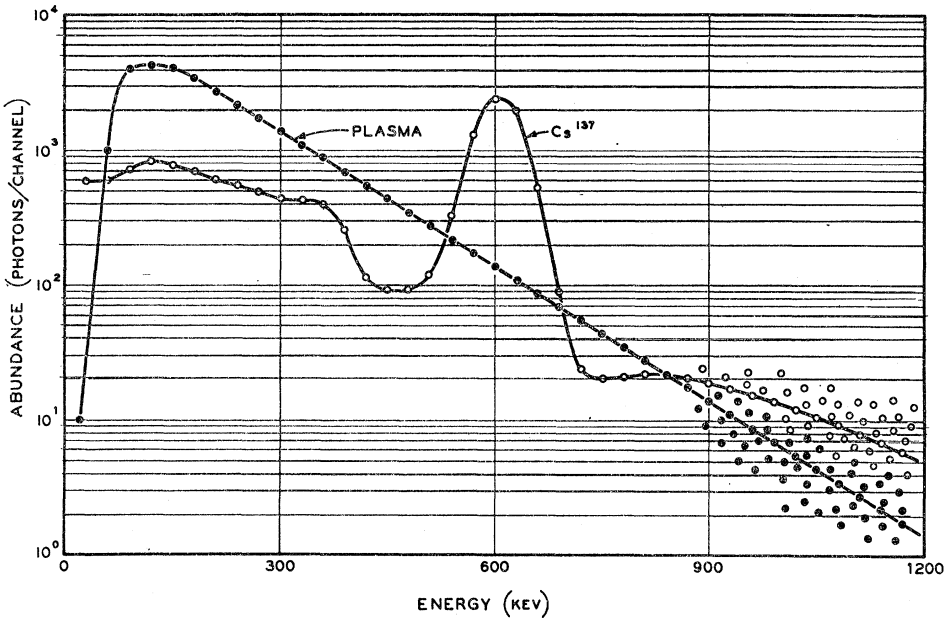

FIG. 2. Energy distribution of x rays from the plasma and from a Cs^{137} source for calibration.

transient in the filament bias circuit. Secondary plasma would form, and it would then remain in a high-resistance mode permitting a fivefold increase (up to 2.5 kW) in power input to the plasma. In this mode the plasma in the mirror throat is almost completely ionized[6] and may extend beyond the anode into the region between the magnetic mirrors.

In practice the magnetic field strength and mirror ratio could be varied over a wide range and still retain some interaction, but there was a "best value" for maximum electron temperature. This will be discussed in connection with a possible resonance between the electron-cyclotron frequency, plasma frequency, and the frequency of a cavity mode involving the coil containers.

Experiment has shown that the high-density plasma in the coil throat next to the cathode may be traversed by ionic sound waves,[5] be fully ionized,[7] and may emit ions random in energy and direction.[4] Electron temperatures of tens of kilovolts have been observed with plasmas of hydrogen, helium, nitrogen, and argon. With deuterium the secondary plasma has been shown to contain trapped deuterium ions of about[6] 70 eV as well.

Our first paper[3] on beam-plasma interaction attributed the plasma electron heating to an instability which produced large amplitude oscillations in the plasma enclosure and electron heating by a cyclotron resonance. However, the enclosure was not a microwave cavity in the strict sense. No effort was made to obtain a high cavity Q. We later removed the entire cylindrical portion of the cavity for photographic and visual observation and could still obtain optimum electron heating. We do not presently understand the heating mechanism, but the following features of the experiment may be pertinent.

The resonant frequency of the cavity in the mode of interest is dependent only on the axial dimension, and this was not altered by removal of the cylindrical portion. It is conceivable that electrons may be heated by a resonance which occurs between a cavity frequency and the electron-cyclotron frequency. For example, the lowest frequency of the fundamental cavity mode was 0.76×10^9 cps, measured experimentally. Many other modes with higher frequencies were possible. The electron-cyclotron frequency at the midplane of the apparatus was about 4×10^9 cps. Since the frequencies of the cavity modes are increased by the presence of the plasma, it is conceivable that even a fundamental mode of the cavity is in resonance with the electron-cyclotron frequency. A resonance with the plasma frequency $(n_e e^2/\pi m_e)^{1/2}=5\times10^9$ cps is also possible.

ELECTRON TEMPERATURE

The total photon flux from the plasma and its energy spectrum were measured by a sodium iodide scintillation crystal, photomultiplier, amplifier, counter, and multichannel analyzer. A sample spectrum is shown in Fig. 2. A calibration spectrum of a Cs^{137} source is shown for comparison. Note that the energy distribution is exponential over three decades, and that some plasma electrons must have energies as great as 1 meV. An additional check by an x-ray absorption technique supported the general features of the energy spectrum. By assuming a point source and isotropic distribution, the total photon flux was conservatively estimated to be

[6] Igor Alexeff, R. V. Neidigh, and E. D. Shipley, Phys. Fluids **6**, 450 (1963).

[7] Igor Alexeff and R. V. Neidigh, Bull. Am. Phys. Soc. **9**, 469 (1964).

10^{10} photons per sec. Electron temperatures may be calculated from the x-ray spectrum by use of known formulas,[8] assuming the plasma is fully ionized. We associate the slope of the exponential section of the x-ray spectrum with $-h\nu/kT_e$ and derive an electron temperature of $T_e=130$ keV.

ELECTRON DENSITY

The electron density n_e can be inferred from the foregoing data by use of the relation $\epsilon=1.42\times10^{-27} n_e n_0 Z^2 T_e^{1/2}$, where the rate of energy emission ϵ takes the value 12 ergs cm^{-3} sec^{-1}, as indicated by the source strength and the energy spectrum (n_e is in cm^{-3}, the gas density n_0 is in cm^{-3} and T_e is in °K). Inserting $Z=1$ (deuterium) and a plasma volume of 100 cm^3, as derived from the pinhole image together with $T_e=130$ keV, we obtain a density value of about $n_e=10^{11}$/cm^3. We believe n_e is nearly correct because (1) an independent neutral beam method is in agreement, and (2) the plasma decay time is often as long as stability and complete purity permit.

The neutral beam measurement of the density of the hot electrons was made by evaporating gold from a filament on one side of the plasma, and measuring the density of the deposited gold in the "shadow" of the plasma on the opposite side. The sketch of Fig. 3 illustrates the method. We analyzed the deposit by light transmission, x-ray fluorescence, and weight of equal areas. Typical distributions of the light transmission and x-ray fluorescence are shown. All methods of analysis gave 1×10^{11} to 2×10^{11} cm^{-3} for the electron density of the most dense region of the plasma.

The light transmission method proved to be the quickest. In this case the electron density was calculated from the equation

$$n_e=\frac{V_m}{\sigma_e V_e D}\ln\left[\frac{\ln(i_0/i_1)}{\ln(i_0/i)}\right].$$

V_m is the thermal velocity of the metal vapor. σ_e is the cross section for ionization by electrons with velocity V_e. D is the diameter of the plasma; i is the light transmission in the plasma shadow; i_1 is out of the shadow, and i_0 is the transmission of a clean plate. All units are expressed in the cgs system. This technique is possible because we assume the product $\sigma_e V_e$ to be essentially constant over the range of interest. The mercury data of Harrison[9] supports this assumption. We apply Harrison's cross-section values for mercury to gold, the next element in the periodic table.

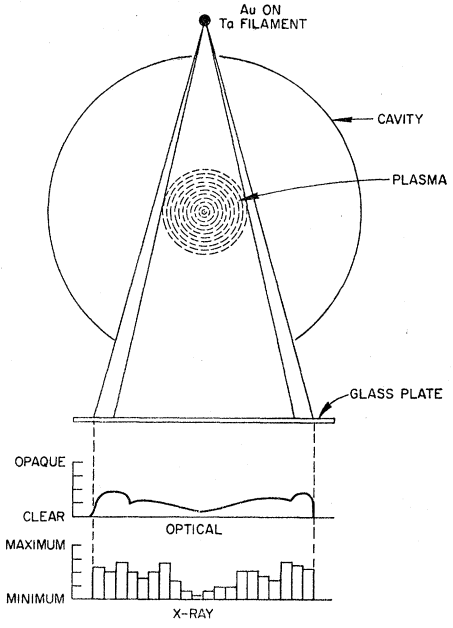

FIG. 3. Method of gold evaporation for determination of electron density. The gold deposit was measured optically, by x-ray fluorescence and by weighing. Typical results are shown. The dips near the edges of the optical scan are apparently due to local crystallization of the gold film.

PLASMA PRESSURE

A minimum value for the plasma pressure may be determined from the decay in its diamagnetism after electron-beam turnoff. A loop of 100 turns and electrostatically shielded was placed around the plasma at the midplane. Although the presence of the loop disturbs the plasma (it shortens its decay time and reduces its temperature), it is an independent measurement and therefore useful. In principle, the voltage developed in the loop after electron-beam turnoff is a measure of the rate of magnetic field change due to the decaying plasma (emf$\sim d\phi/dt$). The two photographs at the left in Fig. 4 show this plasma decay rate ($\tau=0.003$ sec). The indicated change in magnetic field strength in the plasma volume was about 100 G in an applied axial field of 1500 G, giving a plasma pressure to magnetic pressure ratio, $\beta=2\Delta B/B$, greater than 0.1.

Again, the electron density may be calculated since the diamagnetic effect is proportional to $n_e T_e$, and we assume T_e to be known from the photon-energy distribution. It was found to be about 10^{11} cm^{-3}.

A fluctuating plasma pressure was observed in the steady state. The upper traces in the photographs on the right (double exposures) show a fluctuating potential across the loop. By comparison with the known ripple voltage in the coil supply which makes a corresponding ripple in the magnetic-field strength, also seen by the loop (bottom trace, note scale changes), we estimate a maximum field change of about 15 G. Apparently the plasma is expanding and contracting across the loop or

[8] L. Spitzer, Jr., *Physics of Fully Ionized Gases* (Interscience Publishers, Inc., New York, 1956), 1st ed., Chap. 5, p. 88.

[9] H. Harrison, *The Experimental Determination of Ionization Cross Sections of Gases Under Electron Impact* (Catholic University Press, Washington, D. C., 1956).

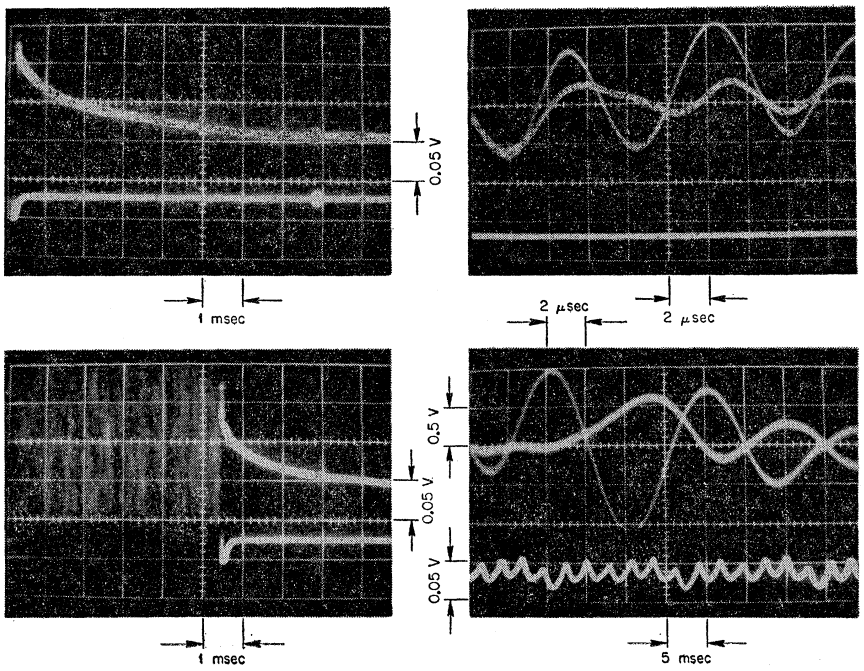

FIG. 4. Plasma diamagnetic effect. Upper trace in each photograph is the voltage developed across a 100-turn loop around the plasma at the midplane.

changing in density within the loop during the steady state. This corresponds to a fluctuating β of about 0.02, and if it is an electron density change, $n_e > 10^{10}$ electrons cm^{-3}.

STABILITY IN THE DECAY

We observed that the plasma decayed with a constant e-folding time, τ(sec) Fig. 5, predictable from the multiple scattering equation

$$\tau = \frac{\theta^2 E^2}{2\pi n_0 v Z^2 e^4 \ln(A_0 E/Z^{4/3}e^2)}.$$

Therefore, the plasma was not thought to be dissipated by instabilities, at least during its decay. In the equation, θ (rad) is the angle through which the velocity vector of an electron initially rotating about the axis must change to reach the loss cone, E is the electron energy (erg), n_0 is the gas density (cm^{-3}), v is the electron velocity (cm sec^{-1}), Z is the atomic number of the background gas (1 for deuterium), e is the electronic charge (esu), and A_0 is the Bohr radius (cm). We assume that Z equals 1 and electron-neutral collisions are the dominating loss mechanism.

The data are shown on a plot of decay time versus electron temperature. The lower solid line of the graph is the calculated decay time for a neutral density of 3.5×10^{12} cm^{-3}. The data points near this line were normalized to this neutral density. We think the scatter above and below the line indicates errors in our measurement of n_0 and of τ.

A better case for the stability of the hot-electron plasma could be made if the neutral density were reduced and the decay time found to be proportionately longer. We did this by a special valving technique, and the data are also given in Fig. 5. The family of curves are the calculated decay times versus electron temperature for the neutral densities indicated. The three points are the measured values of electron temperature and the e-folding time τ of the decay. In general, we see the decay time is proportionately longer as expected, but again the agreement with the scattering equation depends on the accuracy of the n_0 and τ measurements.

Actually, we think the data are in excellent agreement with the value predicted by the multiple scattering equation, and therefore the plasma both shows stability during the decay and is free of high Z contaminants. In order to determine n_0 and τ, it is necessary to understand the method of reducing the neutral pressure.

The method is shown schematically in Fig. 6. An air driven plunger accelerates over a 3-in. travel and plugs the gas flow at the end of its stroke which is adjacent to the defining slot in the mirror throat. Gas flow is stopped in less than a millisecond. Power turnoff is simultaneous. Gas flow through the leak valve is not changed but this gas simply fills the reservoir. The reservoir capacity is large enough to absorb gas for several seconds. At turnoff the 20-in. diffusion pump on the vacuum chamber begins removal of the neutral gas.

If the pump were able to drop the pressure in the apparatus to a very low value, an appreciable part of the hot-electron plasma would be trapped and confined for very long times. This trapping factor can be expressed mathematically as follows: Let τ_a be the time

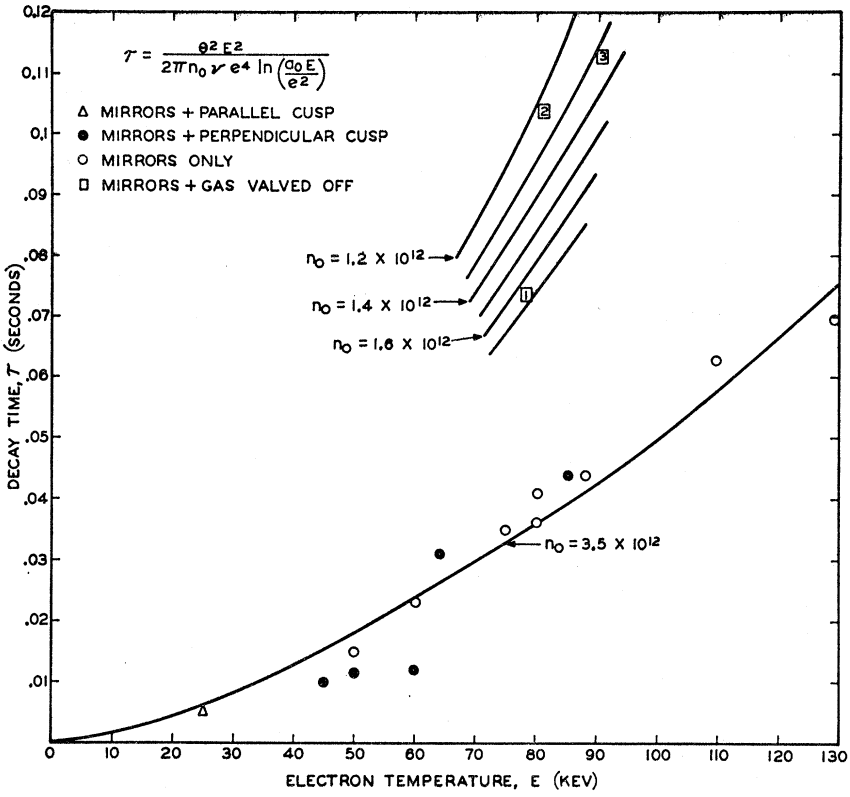

FIG. 5. Decay time versus electron temperature of hot-electron plasma. Solid lines are for different values of neutral density.

in which the plasma density would drop to e^{-1} of its initial value if the gas pressure were kept constant. Let τ_b be the time in which the background gas density drops to e^{-1} of its value after the gas-feed valve is turned off. Then the trapped plasma density n at very long times after gas turnoff (ignoring ion-electron, electron-electron scattering, and instabilities) is given by the following equation: $n=n_0 \exp(-\tau_b/\tau_a)$, where n_0 is the initial plasma density. Thus, under ideal conditions, $\tau_b \ll \tau_a$, most of the hot-electron plasma could be trapped and studied in a high-vacuum environment. Actually, we did not have a low enough ultimate pressure to get very long confinement times, but a big improvement was noted.

The rate of pressure decrease of a vacuum system is

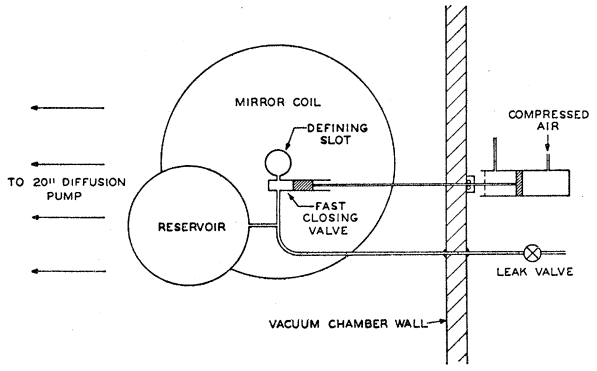

FIG. 6. Schematic diagram of fast closing gas valve. An air driven plunger cuts off gas flow at the defining slot. The reservoir collects gas during a plasma decay.

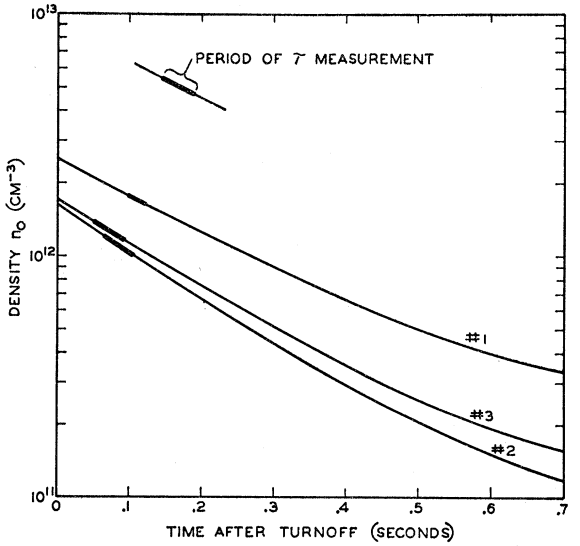

FIG. 7. Neutral density versus time after turnoff. Since the pressure could not be measured during a run the curves were obtained from measured pumping speeds before each run, a typical pressure versus time curve without plasma, and pressure measurement before and after the run.

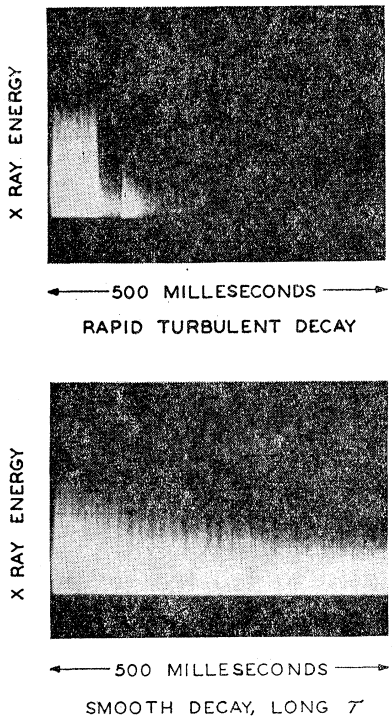

FIG. 8. X-ray flux decay after turnoff. Upper photo shows a rapid, turbulent decay. Lower photo shows smooth decay lasting well over 0.5 sec.

partly dependent on the history of the system and may vary from run to run. The gas handling capacity was measured before each of the three runs and since the rate of pressure decrease could not be measured during a run, the rate of pressure decrease during a trial without plasma was obtained.

Neutral density n_0 versus time after turnoff could now be estimated for the three runs and is shown in Fig. 7. Note how closely the density at which τ was measured agrees with the density in the family of curves of Fig. 5. The τ continued to increase with time as it should, and for run 3 there was sufficient x-ray flux to determine a τ of 0.350 sec after 0.3 sec, and the x-ray flux remained above background for 0.8 sec.

The three runs shown were the most stable observed. We noted that for some combinations of gas-feed rate, magnetic-field strength, mirror ratio, and power input the x-ray output came in bursts during the steady state. We did not consider this a good adjustment of the parameters. Decay of the plasma from this "not so steady" steady-state condition was much more rapid and the x-ray bursts continued during the decay. Two extremes in x-ray output during the decay are shown in Fig. 8. There was some variation in the decay time with the best adjustment of parameters which led us to believe that the decay τ was in some way dependent on the condition of the plasma at turnoff.

ION TEMPERATURE

Ions are warmed by the interaction associated with this method of plasma generation.[4] In the steady state the plasma diameter in the midplane indicates a maximum deuterium ion energy of 1.8 keV for ions passing through the axis. During the decay charge exchange and scattering quickly peg the ion temperature at about 70 eV, as has been shown.

COMMENTS ON STABILITY

We noted the sudden reduction in x-ray output at beam turnoff, as in Fig. 8, on numerous occasions. An explanation for this may be found in the electron temperature. The Debye shielding distance $[6.9(T_e/n_e)^{1/2} = 0.6 \text{ cm}]$ is a large fraction of the diameter (2 cm) of the dense central region. Therefore this part may not be a true plasma but may behave as a collection of independent particles. The outer cooler portions of the plasma may shed quickly after beam turnoff, while the central region with the longer Debye distance may be quite stable. This would account for the sudden drop in x-ray intensity after beam turnoff, but not for x-ray bursts during the decay.

Impurities (high Z components) in the plasma may cause the frequent rapid turbulent decay. The logarithmic factor in the scattering equation may be written

$$\ln A_0 E\epsilon^{-2} - \ln Z^{4/3}.$$

Note that if impurities are present the value of the Z term may dominate if E is small or if E decreases during the decay. The diamagnetic probe indicated a "sloshing" of the plasma with beam on, and it is quite possible that impurities may enter the plasma region in an unsteady way from plasma contact with a wall giving rise to the x-ray bursts during decay.

Another argument for stability in the decay is the behavior of τ as a function of n_0. If we select the data which gave the longest decay times and plot $1/\tau$ versus n_0, we find extrapolation to zero pressure gives an infinite decay time $(1/\tau = 0)$, Fig. 9. The plasma always appears noisy in the steady state to both electrostatic and magnetic probes. This may be due to the high beta. As the plasma decays, the noise abates. Even in the long

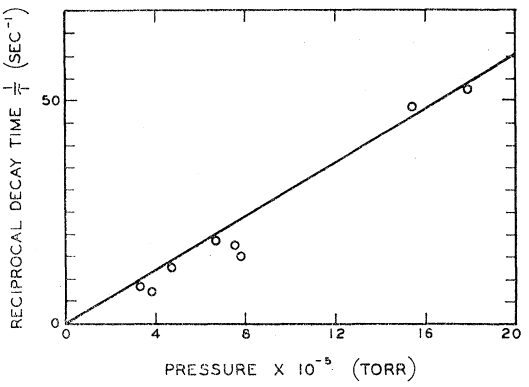

FIG. 9. Reciprocal decay time versus neutral pressure. Note extrapolation goes through origin.

smooth decay in Fig. 8, some structure can be seen in the x-ray flux.

We feel that the stabilizing effect of hot electrons should not be overlooked in the planning of thermonuclear experiments.

Note added in proof. A lower limit to the heating efficiency of the electron beam is easily calculated, and is found to be surprisingly high. The heating efficiency is defined as the ratio of the steady-state loss of power from the plasma to the input power of the beam. A lower limit to the power loss from the plasma is given by the total energy stored in the plasma divided by its decay time constant. Any instability during steady-state operation would cause the plasma to be lost faster, and give a larger value to the power loss. An upper limit to the power input is the power drain on the power supply. Since some of the electron beam does not pass through the hollow anode and does not reach the plasma, this number is too big. The largest ratio of these two numbers is found in the short-lifetime experiments using the diamagnetic loop. Here the lower limit to the heating efficiency is about one percent.

ACKNOWLEDGMENTS

We wish to thank our associates in the Thermonuclear Division for their criticism and encouragement, the laboratory administration for its support, and J. G. Harris whose technical skill made these experiments possible.

PHYSICAL REVIEW VOLUME 136, NUMBER 3A 2 NOVEMBER 1964

Magnetic Properties of the Canted Antiferromagnet α-$CoSO_4$†

I. F. SILVERA, J. H. M. THORNLEY,* AND M. TINKHAM
Department of Physics, University of California, Berkeley, California
(Received 27 May 1964)

It is known from neutron scattering experiments that α-$CoSO_4$ is a four-sublattice canted antiferromagnet with no net magnetic moment. In this paper the magnetic properties of this material are analyzed using a model in which an isotropic fictitious spin of $\frac{1}{2}$ is assigned to each Co^{++} ion. The large canting angle of 25° is interpreted in terms of antisymmetric terms in the Hamiltonian due to anisotropic superexchange and the large anisotropy in the g values. Corresponding to the four sublattices, there are four spin-wave modes at $k=0$. Calculations indicate that the resonant frequencies of these modes should lie in the far infrared, and that only three of the modes should be observable spectroscopically. In addition, static susceptibilities of the system have been calculated for $T=0$ and $T\gg T_N$ (12°K), and the g values have been estimated. Far-infrared transmission experiments have resulted in the observation of three lines at 20.6, 25.4, and 35.8 cm^{-1}, with relative intensities 1:1:0.1. Although these lines are presumed to be the three expected resonances, an unambiguous fitting for all the parameters of the model has not been possible. The temperature dependence of the resonance lines is anomalous.

I. INTRODUCTION

FOR several years there has been much interest in canted magnetic systems. Purely on grounds of symmetry and the thermodynamics of phase transitions, Dzialoshinski[1] first suggested the form of the interaction which gives rise to the canting. Moriya[2] included the effect of spin-orbit coupling in the superexchange Hamiltonian of a system with a nondegenerate orbital ground state to find, in addition to the usual isotropic exchange and the well-known symmetric anisotropic exchange (which finds its origin in the combined effects of the spin-orbit coupling and the crystal field), that there is a further exchange term which is antisymmetric with respect to the interacting spins $\mathbf{S}_i$ and $\mathbf{S}_j$ and is of the form

$$\mathcal{H}_m=\mathbf{D}_{ij}\cdot\mathbf{S}_i\times\mathbf{S}_j. \quad (1)$$

Here $\mathbf{D}_{ij}$ is a vector that depends linearly on the spin-orbit coupling constant, the precise form being derived in Moriya's paper. In most of the canted antiferromagnetic crystals which have been investigated, for example, α-Fe_2O_3,[1] $MnCO_3$,[3] $KMnF_3$,[4] and $CuCl_2\cdot 2H_2O$,[2] the canting angle has been found to be of the order of 1°.

α-$CoSO_4$ has an orthorhombic crystal structure and a four-sublattice canted antiferromagnetic structure having zero net magnetic moment. Its magnetic structure was first determined in the neutron diffraction experiment of Frazer and Brown.[5] They, however, were not at the time of their first paper, aware of the existence of the two forms of $CoSO_4$ (see Sec. III), as they attempted to explain the static susceptibility measure-

† Supported in part by the U. S. Office of Naval Research, The National Science Foundation, and the Alfred P. Sloan Foundation.
* Present address: Clarendon Laboratory, Oxford, England.
[1] I. Dzialoshinski, Phys. Chem. Solids 4, 241 (1958).
[2] T. Moriya, Phys. Rev. 120, 91 (1960).
[3] A. S. Borovik-Romanov, Zh. Eksperim. i Teor. Fiz. 36, 539 (1959) [English transl.: Soviet Phys.—JETP 9, 539 (1959)].
[4] A. J. Heeger, Olaf Beckman, and A. M. Portis, Phys. Rev. 123, 1652 (1961).
[5] B. C. Frazer and P. J. Brown, Phys. Rev. 125, 1283 (1962); P. J. Brown and B. C. Frazer, *ibid.* 129, 1145 (1963).

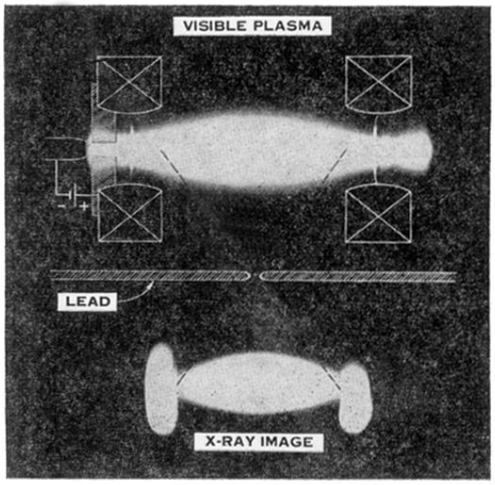

FIG. 1. Visible hot-electron plasma and its x-ray image. Superimposed outline shows magnet coils and electron-beam defining aperture. Dumbbell-like ends on the image are caused by x-ray fluorescence at the magnetic-mirror throat.

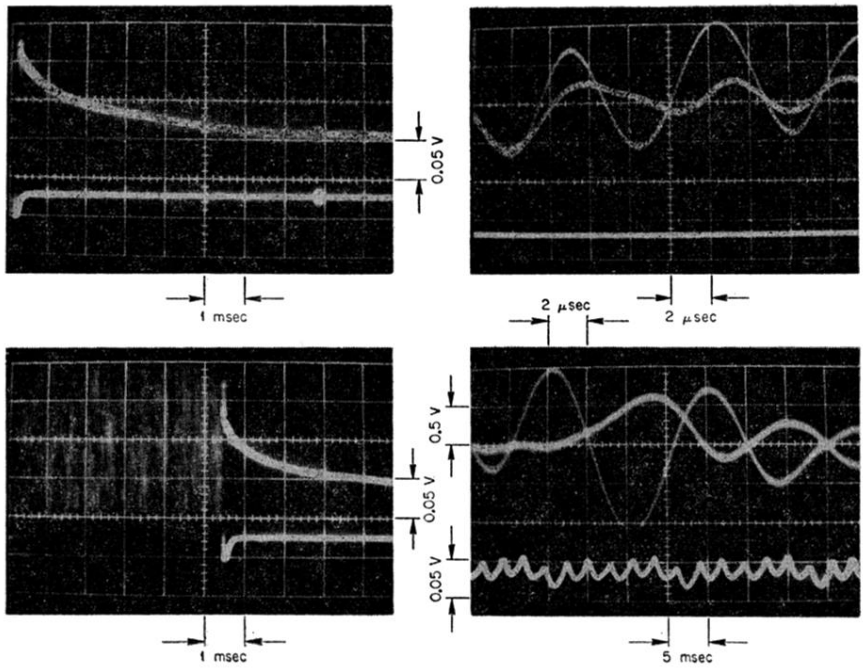

FIG. 4. Plasma diamagnetic effect. Upper trace in each photograph is the voltage developed across a 100-turn loop around the plasma at the midplane.

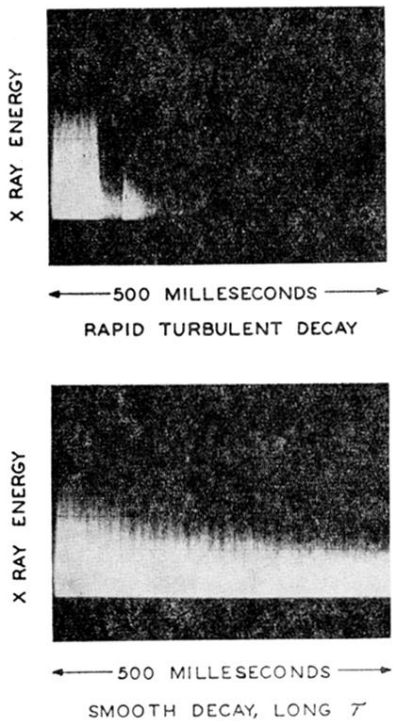

FIG. 8. X-ray flux decay after turnoff. Upper photo shows a rapid, turbulent decay. Lower photo shows smooth decay lasting well over 0.5 sec.